arXiv:1603.07546v2 [quant-ph] 30 Jun 2016

Method for observing robust and tunable phonon blockade in a nanomechanical resonator coupled to a charge qubit

Xin Wang[1,2], Adam Miranowicz[3,2], Hong-Rong Li[1], and Franco Nori[2,4]
[1] *Institute of Quantum Optics and Quantum Information, School of Science, Xi'an Jiaotong University, Xi'an 710049, China*
[2] *CEMS, RIKEN, Wako-shi, Saitama 351-0198, Japan*
[3] *Faculty of Physics, Adam Mickiewicz University, 61-614 Poznań, Poland*
[4] *Physics Department, The University of Michigan, Ann Arbor, Michigan 48109-1040, USA*
(Dated: July 1, 2016)

Phonon blockade is a purely quantum phenomenon, analogous to Coulomb and photon blockades, in which a single phonon in an anharmonic mechanical resonator can impede the excitation of a second phonon. We propose an experimental method to realize phonon blockade in a driven harmonic nanomechanical resonator coupled to a qubit, where the coupling is proportional to the second-order nonlinear susceptibility $\chi^{(2)}$. This is in contrast to the standard realizations of phonon and photon blockade effects in Kerr-type $\chi^{(3)}$ nonlinear systems. The nonlinear coupling strength can be adjusted conveniently by changing the coherent drive field. As an example, we apply this model to predict and describe phonon blockade in a nanomechanical resonator coupled to a Cooper-pair box (i.e., a charge qubit) with a linear longitudinal coupling. By obtaining the solutions of the steady state for this composite system, we give the conditions for observing strong antibunching and sub-Poissonian phonon-number statistics in this induced second-order nonlinear system. Besides using the qubit to produce phonon blockade states, the qubit itself can also be employed to detect blockade effects by measuring its states. Numerical simulations indicate that the robustness of the phonon blockade, and the sensitivity of detecting it, will benefit from this strong induced nonlinear coupling.

PACS numbers: 42.50.Dv, 85.85.+j, 03.65.Yz

I. INTRODUCTION

Quantum mechanics enables many breakthroughs that classical physics cannot reach. However, due to decoherence, there exist huge obstacles when quantum theory is applied to macroscopic systems. In recent years, nanomechanical fabricating technologies have achieved tremendous progress and provide ideal platforms to explore fundamental questions in quantum mechanics. Many efforts [1–5] have been made to approach the quantum limits of nanomechanical resonators (NAMRs), for instance, ground-state cooling [5, 6] and preparing nonclassical states (examples including superposition states [7, 8], squeezed states [9–11], etc).

In experimental implementations, the fundamental frequencies of NAMRs range from tens of Hz to several GHz, and as a result, the thermal environment significantly affects the coherences of mechanical modes. For NAMRs at microwave frequencies [12], the quantum limit can be approached via cryogenic means (in the range of ∼mK). If the energies of mechanical quanta (phonons), are larger than their thermal energy, the quantum behavior of mechanical modes might be observed. However, for mechanical modes of much lower frequencies, the quantum coherences are fragile to thermal environments. Usually, NAMRs need to be cooled to reach their ground states via methods such as side-band cooling [13–15] or active feedback cooling [16, 17]. To operate the mechanical motions effectively, NAMRs are often combined with other systems to form hybrid systems. Examples include optomechanical systems [5, 18] and quantum electromechanical systems [2, 19]. In the quantum regime, NAMRs can be employed in fields such as quantum information processing [20] and quantum metrology [21, 22].

A. Obstacles for observing robust phonon blockade

Phonon blockade (PB) [23–25] is another purely quantum phenomenon, in which a single phonon in a resonator can impede the transmission of a second one. Phonon blockade is an analog of another quantum phenomenon named photon blockade (see Refs. [26–31] and references therein). The interest in photon blockade is also motivated for realizing single-photon sources for quantum-information processing. Compared with classical states, phonon and photon blockade states are described by the sub-Poissonian distribution and can be interpreted as nonlinear quantum scissors [27, 32]. Photon blockade has theoretically been predicted in various systems and was first observed in an optical cavity coupled to a single trapped atom [33]. However, realizing and observing PB are still challenging for the following reasons: (1) The key point for conventional phonon (photon) blockade is the realization of a large nonlinearity with respect to the decay rate of the system. However, moving into the strong nonlinear regime often requires strict conditions which are hard to realize in most systems. (2) The quantum coherence for NAMRs is very easy to be destroyed by any noisy thermal environment. (3) Detecting PB directly is also challenging: The position displacement for

NAMRs is too tiny to be detected effectively under current experimental techniques [23, 24, 34]. Moreover, the zero-point fluctuations for massive objects will limit the measurement accuracy.

To date, most of the studies on phonon and photon blockade are mainly based on nonlinearity (Kerr-type third-order $\chi^{(3)}$ nonlinearity [23, 25–27] and second-order $\chi^{(2)}$ nonlinearity [30, 35, 36]) and quantum interference effects [30, 37]. Phonon and photon blockade in $\chi^{(2)}$ and $\chi^{(3)}$ nonlinear systems both originate from the energy-level shift of multi-excitation states. To observe the blockade of the second excitation, the decoherence rate should be much smaller than the nonlinear strength. Phonon and photon blockade can also be generated by utilizing optimal conditions for quantum interference: transition paths for the multi-excitation states are destructive and will cancel each other, leading to a small population of the second excitation. Recently, a new mechanism called unconventional photon blockade has been predicted [38–42], in which strong two-qubit entanglement and strong photon antibunching can be observed via the destructive quantum interference effect even in the weak nonlinear regime. Reference [37] theoretically proposes how to realize photon blockade via quantum interference effects in a quantum-dot cavity (without any nonlinearity). However, to avoid multiexcited states, the strengths and relative phases of the drive fields must be perfectly fixed when employing quantum interference to prepare blockade states.

B. Summary of our proposal

It should be noted that the nonlinearity can be intrinsic or induced via ancillary systems [23, 25, 43]. Phonon blockade in a Kerr-type nonlinear system has been demonstrated in Refs. [23–25]. Inspired by these works, our goal in this paper is to study PB via an effective second-order nonlinear coupling, which remains unexplored. To obtain a second-order nonlinear coupling, a NAMR is assumed to be coupled to a Cooper-pair box (i.e., a charge qubit) [19, 44, 45] with a linear longitudinal coupling (σ_z coupling) [46–48]. As discussed in Refs. [49–52], coupling a resonator with a superconducting qubit of longitudinal form will induce multiphonon (multiphoton) processes.

It is worth stressing that our system is based on the longitudinal coupling, instead of the transverse coupling assumed in the Rabi model under the rotating-wave approximation. To our knowledge, all former papers on phonon blockade have been based on the Jaynes-Cummings model in the dispersive limit (i.e., assuming large detuning). Our proposal, in which a strong quadratic coupling between the charge qubit and the NAMR can be induced by choosing appropriate driving parameters of the charge qubit, has the following advantages:

(1) The intrinsic and induced effective $\chi^{(3)}$ nonlinearities are usually very weak (about three orders lower of magnitude than the Jaynes-Cummings coupling strength) [25, 28, 53, 54]. However, in this longitudinal-coupling system, the second-order nonlinear strength can be much stronger and, as a result, we can observe robust PB using lower-order nonlinear interactions.

(2) Besides using the qubit to produce PB states, the qubit itself can also be employed to detect PB.

(3) Comparing with the direct nonlinear coupling between a qubit and a NAMR [55], this type of effective coupling does not require the qubit and the NAMR to be resonant, and the effective coupling strength can be adjusted by controlling the strength of the drive field or the longitudinal coupling strength.

In this paper, we first describe the model Hamiltonian in Sec. II. Then, in Sec. III, we obtain the theoretical results for steady states and give conditions to observe strong sub-Poissonian phonon statistics and strong phonon antibunching in our proposal. In Sec. IV, we demonstrate our numerical results and discuss how to increase the robustness against different types of noise in this composite system. In Sec. V, we propose a method to detect PB in this setup. Section VI presents the conclusions.

II. MODEL

A. Hybrid system to generate phonon blockade

The proposed setup is illustrated in Fig. 1. A lossless NAMR (with a fundamental frequency ω_0, an effective length L, and a mass m) is coupled to a charge qubit by applying a static voltage V_0 through a capacitance $C_0(x)$ [56–58]. Around its equilibrium position, $x = 0$, $C_0(x)$ depends on the displacement x of the NAMR, and the distance between the charge qubit and NAMR is d. The tunneling energy and capacitance of two Josephson junctions in a superconducting quantum interference device (SQUID) are E_J and C_J, respectively. The charge states of the qubit can be precisely tuned by adjusting the gate voltage V_g and the static voltage V_0. The driving force for the NAMR is induced by a time-dependent current $I(t) = I_0\cos(\omega_f t)$ and a perpendicular static magnetic field B_0 [23]. The magnetic flux Φ_x through the SQUID loop is produced by the microwave field in the microwave line. Thus, we express the Hamiltonian of the total system as

$$H_{\rm total} = H_{\rm Q} + H_{\rm NAMR}, \tag{1}$$

$$H_{\rm Q} = 2E_c\left(2n_g-1\right)\sigma_z - E_J\cos\left(\frac{\pi\Phi_x}{\Phi_0}\right)\sigma_x, \tag{2}$$

$$H_{\rm NAMR} = \hbar\omega_0 b^\dagger b + \hbar\epsilon\left(b^\dagger + b\right)\cos\left(\omega_f t\right), \tag{3}$$

where $H_{\rm Q}$ is the Hamiltonian of the charge qubit. In the neighborhood of the charge-degeneracy point $n_g = [C_gV_g + C_0(0)V_0]/(2e) \simeq 0.5$, the dephasing noise on the qubit will be suppressed. The charge qubit can be

characterized by the pseudospin Pauli operators $\sigma_z = |e\rangle\langle e| - |g\rangle\langle g|$ and $\sigma_x = \sigma_+ + \sigma_- = |e\rangle\langle g| + |g\rangle\langle e|$, with $|e\rangle$ ($|g\rangle$) being the excited (ground) state for the qubit. Here $H_{\rm NAMR}$ is the Hamiltonian for the driven mechanical mode of the NAMR, and $b^\dagger$ and b are the phonon creation and annihilation operators, respectively. We define $\hbar\omega_{\rm q}$=$4E_c\,(2n_g-1)$, with $E_c = e^2/\,(2C_\Sigma)$ being the charging energy of the qubit with the total capacitance $C_\Sigma = C_J + C_0(0) + C_g$ (we assume that $C_0(0)$ and C_g are much less than C_J). The displacement x of the NAMR gives rise to the linear modulation of the capacitance between the NAMR and Cooper-pair box island, that is, $C_0(x) = C_0(0)\,(1 - x/d)$. This leads to the coupling constant

$$g = \frac{2E_cC_0(0)V_0}{ed\hbar}X_0, \tag{4}$$

where $X_0 = \sqrt{\hbar/\,(2m\omega_0)}$ describes the zero-point fluctuations of the NAMR. The parameter

$$\epsilon = \hbar^{-1}B_0I_0LX_0 \tag{5}$$

is the driving strength of the Lorentz force for the NAMR, which is induced by an alternating current at a frequency ω_f and a static magnetic field B_0.

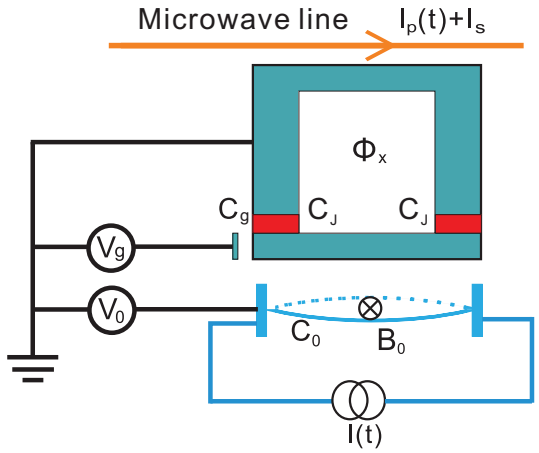

FIG. 1: (Color online) Schematic diagram of the coupled system of a NAMR and a Cooper-pair box working as a charge qubit. The two Josephson junctions (red rectangles) with tunneling energy E_J and capacitance C_J form a SQUID loop. The perpendicular static magnetic field B_0, together with the current $I(t)$ through the NAMR, produces the Lorentz force to drive the NAMR. Here a gate voltage V_g and a static voltage V_0 are applied to the capacitances C_g and C_0, respectively. The microwave line is located right above the charge qubit. The time-dependent current $I_{\rm p}(t)$ and static current $I_{\rm s}$ in the microwave line induce a magnetic flux Φ_x through the SQUID loop.

The second term in $H_{\rm Q}$ is the Josephson energy. Here $\Phi_0 = \hbar/\,(2e)$ is the flux quantum. The coupling between the microwave line and the qubit results from the magnetic flux

$$\Phi_x = M[I_{\rm p}(t) + I_{\rm s}] \tag{6}$$

applied through the SQUID loop via the mutual inductance M. Here $I_{\rm p}(t) = \varepsilon_{\rm p}\cos(\omega_{\rm p}t)$ and $I_{\rm s}$ are the time-dependent and direct current in the microwave line, respectively. Under the conditions $MI_{\rm s} = \Phi_0/2$ and $I_{\rm p}(t) \ll I_{\rm s}$, we expand the Josephson energy to first order as $E_J\sigma_x \sin y \approx E_Jy\sigma_x$, where $y = \pi MI_{\rm p}(t)/\Phi_0 \ll 1$. Applying a frame rotating at a frequency $\omega_{\rm p}$ and adopting the rotating wave approximation, the Hamiltonian of the total system becomes (setting $\hbar = 1$)

$$\begin{aligned} H_{\rm total} = &\frac{1}{2}\Delta\sigma_z + \omega_0 b^\dagger b + g\sigma_z(b^\dagger + b) \\ &+ \Omega_{\rm p}\,(\sigma_+ + \sigma_-) + \epsilon\left(b^\dagger e^{-i\omega_f t} + be^{i\omega_f t}\right), \end{aligned} \tag{7}$$

where $\Delta = \omega_{\rm q} - \omega_{\rm p}$ is the drive-excitation detuning and

$$\Omega_{\rm p} = \frac{\pi E_J M I_{\rm p}(t)}{\hbar\Phi_0} \tag{8}$$

is the effective Rabi frequency of the drive field.

B. Induced nonlinear qubit-NAMR coupling

To achieve the nonlinear coupling, we set the driving field for the qubit as red sideband with $\Delta \simeq 2\omega_0$, as shown in Fig. 2(a) (black arrows). Moreover, we do not consider the weak drive ϵ of the NAMR at the beginning. Performing the polariton transformation [50, 59, 60] to $H_{\rm total}$

$$\tilde{H} = e^S H_{\rm total}\, e^{-S} \tag{9}$$

with $S = \beta\sigma_z(b^\dagger - b)$ and $\beta = g/\omega_0$, we obtain

$$\tilde{H} = \frac{1}{2}\Delta\sigma_z + \omega_0 b^\dagger b + [\Omega_{\rm p}\sigma_+ e^{2\beta(b^\dagger - b)} + {\rm H.c.}], \tag{10}$$

where H.c. denotes the Hermitian conjugate of the last term in $\tilde{H}$. In this shifted oscillator framework, we expand the above equation to second order in the small parameter β, and we obtain

$$\begin{aligned} \tilde{H} = &\frac{1}{2}\Delta\sigma_z + \Omega_{\rm p}(\sigma_+ + \sigma_-) + \omega_0 b^\dagger b \\ &+ 2\Omega_{\rm p}[\beta\sigma_+(b^\dagger - b) + {\rm H.c.}] \\ &+ 2\Omega_{\rm p}[\beta^2\sigma_+(b^\dagger - b)^2 + {\rm H.c.}]. \end{aligned} \tag{11}$$

The second term in Eq. (11) will cause the dynamical energy shifts for the charge qubit. Defining the shifted energy as

$$\tilde{\Delta} = \sqrt{\Delta^2/4 + \Omega_{\rm p}^2}, \tag{12}$$

and expressing the new eigenstates in the basis of the charge states

$$\begin{aligned} |-\rangle &= \cos\frac{\theta}{2}|g\rangle - \sin\frac{\theta}{2}|e\rangle, \\ |+\rangle &= \sin\frac{\theta}{2}|g\rangle + \cos\frac{\theta}{2}|e\rangle \end{aligned} \tag{13}$$

with $\tan\theta = 2\Omega_{\rm p}/\Delta$, we rewrite $\tilde{H}$ as

$$\begin{aligned}\tilde{H} = &\tilde{\Delta}\tilde{\sigma}_z + \omega_0 b^\dagger b + 2\lambda\Omega_{\rm p}(\tilde{\sigma}_+ - \tilde{\sigma}_-)(b^\dagger - b) \\ &+ 2\Omega_{\rm p}\lambda^2 \sin\theta\tilde{\sigma}_z(b^\dagger - b)^2 \\ &+ 2\Omega_{\rm p}\beta^2\cos\theta(\tilde{\sigma}_+ + \tilde{\sigma}_-)(b^\dagger - b)^2,\end{aligned} \tag{14}$$

where $\tilde{\sigma}_z = |+\rangle\langle+| - |-\rangle\langle-|$, $\tilde{\sigma}_+ = |+\rangle\langle-|$ and $\tilde{\sigma}_- = |-\rangle\langle+|$. The driving for the qubit is far detuned with $\Delta \gg \Omega_{\rm p}$, so the rotating angle θ of the new basis is very small, and we have $\sin\theta \simeq \Omega_{\rm p}/\omega_0 \ll 1$ and $\cos\theta \simeq 1$. The third and forth terms in Eq. (14) represent the energy shifts for the qubit and the NAMR. Assuming that the qubit is approximately in its ground state ($\sigma_z = \tilde{\sigma}_z = -1$, since the sideband driving is far detuned), the renormalized NAMR frequency can be expressed by

$$\omega_0' = \omega_0 - \frac{4\Omega_{\rm p}^2\lambda^2}{3\omega_0^3}, \tag{15}$$

where the second term in this equation describes the eigenfrequency shift of the NAMR [57]. In this paper, we consider the resonant case $\tilde{\Delta} = \omega_0'$ and assume the parameters satisfy the condition

$$\Delta \simeq 2\omega_0 \gg \max\{g, \Omega_{\rm p}\} \geq \min\{g, \Omega_{\rm p}\} \gg \epsilon, \tag{16}$$

Performing the unitary transformation

$$U = \exp[-i(\tilde{\Delta}\tilde{\sigma}_z + \omega_0' b^\dagger b)t] \tag{17}$$

of $\tilde{H}$ in Eq. (14), we can neglect the rapid oscillating terms and obtain the effective Hamiltonian as follows

$$\tilde{H} = \lambda(\tilde{\sigma}_+ b^2 + \tilde{\sigma}_- b^{\dagger 2}). \tag{18}$$

where

$$\lambda = \frac{2\Omega_{\rm p} g^2}{\omega_0^2} \tag{19}$$

is the effective nonlinear coupling strength between the states $|g, n+2\rangle$ and $|e, n\rangle$, where the $|n\rangle$ are the Fock states of the mechanical mode. Equation. (18) describes a nonlinear process that the qubit can be excited by the annihilation of two phonons, or the inverse process as shown in Fig. 2(b).

It should be noted that $\tilde{H}$ in Eq. (18) is the Hamiltonian after performing the small polariton transformation and rotating the qubit basis with an angle θ, so the evolution of the density matrix $\tilde{\rho}(t)$, described by $\tilde{H}$, is also in the rotating frame. In fact, we are ultimately interested in the dynamics as seen in the original non-transformed lab frame $\rho(t)$. To obtain a complete description of the system, we also need to apply these two rotating transformations to the bath-system coupling. In principle, this can be done by transforming the operators in the master equation. Only after these two steps we can obtain the explicit solutions to this system. However, here we have assumed that both of these two transformations just *slightly* rotate the density matrix under the small parameters β and θ, so $\tilde{\rho}(t)$ can be viewed as an approximate solution for $\rho(t)$. For the collapse operators in the master equation, we can also neglect the terms of order λ and θ. We find that these assumptions to be valid by comparing our theoretical and numerical results.

By including the drive of the NAMR, the effective Hamiltonian of the system can be expressed as

$$H_{\rm eff} = \lambda(b^2\sigma_+ + b^{\dagger 2}\sigma_-) + \epsilon(b^\dagger e^{i\Delta_d t} + be^{-i\Delta_d t}), \tag{20}$$

where $\Delta_d = \omega_0' - \omega_f$ is the detuning between the renormalized NAMR frequency, given by Eq. (15), and the frequency ω_f of the alternating current $I(t)$. Assuming $g = \Omega_{\rm p} = 0.1\omega_0$, a strong nonlinear coupling with strength $\lambda = \omega_0/500$ can be achieved. Defining the time-dependent probabilities P_{ij} ($i = 0, 1, 2...$ and $j = g, e$) for the states $|j, i\rangle$ and setting $\epsilon = 0$, we numerically solve the Schrödinger equation governed by $H_{\rm total}$ with the initial state $|e, 0\rangle$, and plot the results in Fig. 2(d). We find that the amplitudes of P_{0e} and P_{2g} approximately exhibit Rabi oscillations with the Rabi frequency $\sqrt{2}\lambda$.

Thus, under the appropriate red-sideband driving for the qubit, we realize an effective nonlinear coupling between the NAMR and the qubit. Different from the direct nonlinear coupling proposal in Ref. [55], the induced nonlinear coupling described here should be easier to realize in experiments. In this work, we consider a pseudospin charge qubit coupling with a NAMR of the longitudinal form just as an example, but the same coupling also exists between mechanical modes and a semiconductor quantum dot [59] (or a carbon nanotube [60], an electronic-spin qubit [61], etc.). Thus, our discussions in this paper can also be applied to those systems.

III. ANALYTICAL DESCRIPTION OF PHONON BLOCKADE

Once the effective nonlinear coupling in Eq. (20) is induced, the ground state is $|g, 0\rangle$ and the first-excited state is $|g, 1\rangle$. However, the second excited states are the superposition states of $|g, 2\rangle$ and $|e, 0\rangle$ with splitting $2\sqrt{2}\lambda$. The energy-level diagrams for the first few excitation states can be found analytically as shown in Fig. 2(b, c). Hence, when the NAMR is driven by a resonant force with strength ϵ (red solid line in Fig. 2), the first phonon of the NAMR can be easily generated, while the second phonon can be hardly excited, since there are no corresponding transmission energy levels for the second incoming phonon. Thus, the second phonon is blocked by the first incoming phonon.

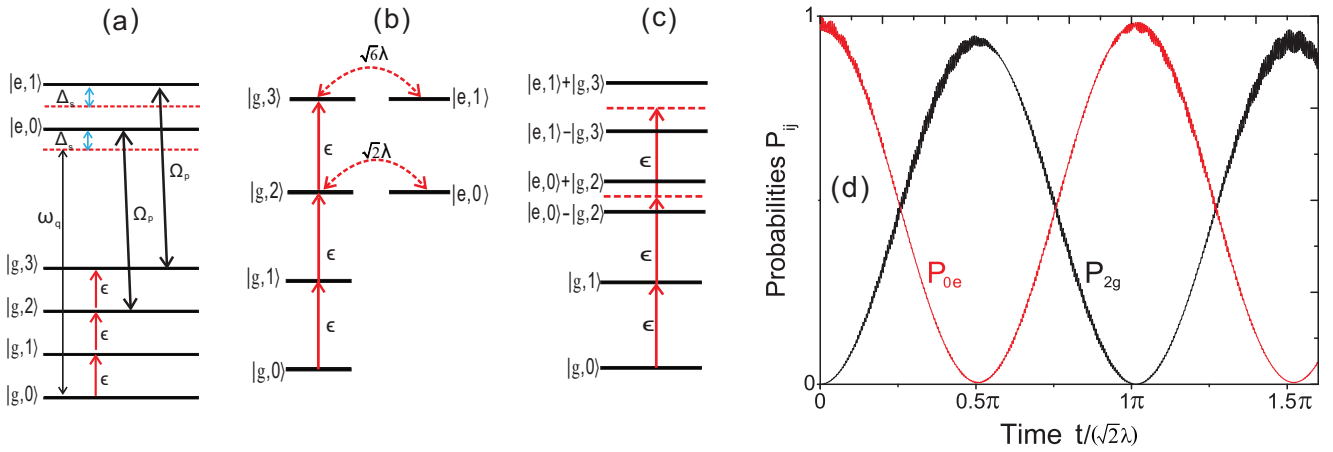

FIG. 2: (Color online) Schematic energy-level diagrams [in (a), (b), and (c)] explaining the occurrence of phonon blockade in our approach. The red and black arrows represent the drivings for the NAMR and qubit with strengths ϵ and $\Omega_{\rm p}$, respectively. (a) The energy shift $\Delta_s = \tilde{\Delta} - \Delta$ (blue two-direction arrows) of the energy gap for the qubit is due to the side-band driving. (b) The induced nonlinear strength λ leads to the transfer between states $|e,0\rangle \leftrightarrow |g,2\rangle$ ($|e,1\rangle \leftrightarrow |g,3\rangle$) with rate $\sqrt{2}\lambda$ ($\sqrt{6}\lambda$). (c) Due to the energy level splitting between the dressed states $(|e,n\rangle \pm |g,n+2\rangle)/\sqrt{2}$, there is no corresponding transition level for a multiphonon being excited. (d) The time evolution of the probabilities P_{2g} (black curve) and P_{0e} (red curve) demonstrate the Rabi oscillations between the states $|g,2\rangle$ and $|e,0\rangle$ without considering any decay channels.

However, for a strong driving rate of the NAMR, high excitation states might become occupied and the blockade effect will be weaker. Moreover, the decoherences of the qubit and the NAMR also lead to the deterioration of PB. In this section, we will derive the expression of the second-order correlation function $g_2(0)$ under the low-excitation approximation, and give the conditions for observing strong antibunching and sub-Poissonian phonon statistics effects.

First we analyze the steady state of our system by analyzing non-Hermitian Hamiltonians.

A. Steady-state solutions of the Schrödinger equation for the non-Hermitian Hamiltonian

If we assume that the driving strength ϵ is much smaller than the effective nonlinear coupling strength λ, then we can conjecture that the infinite-dimensional mechanical-mode Hilbert space can be reduced into the two-phonon excitation subspace. Then we can expand the wave function in the basis spanned by $\{|g,0\rangle, |g,1\rangle, |e,0\rangle, |g,2\rangle\}$ as follows:

$$|\psi\rangle = C_{0g}|g,0\rangle + C_{1g}|g,1\rangle + C_{0e}|e,0\rangle + C_{2g}|g,2\rangle, \quad (21)$$

with $|C_{ij}|^2 = P_{ij}$, which is a good approximation to describe phonon blockade. The validity of this approximation will be discussed in Sec. IV, e.g., in the analysis of Fig. 4. With the assumption $\Delta_d = 0$, the decay of the charge qubit and the mode loss can be treated by the non-Hermitian time-independent Hamiltonian

$$H_{\rm nH} = H_{\rm eff} - i\frac{\kappa}{2}b^\dagger b - i\frac{\Gamma}{2}|e\rangle\langle e|, \quad (22)$$

where we have assumed that the qubit and the NAMR couple with the vacuum reservoirs, and the corresponding damping rates are Γ and κ, respectively. Substituting the state $|\psi\rangle$ and $H_{\rm nH}$ to the Schrödinger equation, we obtain the equations of motion for the coefficients in Eq. (21):

$$\begin{aligned} i\frac{\partial}{\partial t}C_{1g} &= \epsilon C_{0g} - i\frac{\kappa}{2}C_{1g} + \sqrt{2}\epsilon C_{2g}, \\ i\frac{\partial}{\partial t}C_{2g} &= \sqrt{2}\epsilon C_{1g} - i\kappa C_{2g} + \sqrt{2}\lambda C_{0e}, \\ i\frac{\partial}{\partial t}C_{0e} &= \sqrt{2}\lambda C_{2g} - i\frac{\Gamma}{2}C_{0e}. \end{aligned} \quad (23)$$

By setting $\partial C_{ij}/\partial t = 0$ (i =0, 1, 2 and j=g, e), we obtain the steady-state solution for each coefficient:

$$C_{0e} = \frac{2\sqrt{2}\lambda}{i\Gamma}C_{2g}, \quad (24a)$$

$$C_{2g} = \frac{\sqrt{2}\epsilon}{i\left(2\kappa + \frac{4\lambda^2}{\Gamma}\right)}C_{1g}, \quad (24b)$$

$$C_{0g} = \frac{i\kappa}{2\epsilon}C_{1g} - \sqrt{2}\epsilon C_{2g}. \quad (24c)$$

For a strong phonon blockade effect, the NAMR is treated as a two-level system while multiphonon states ($n \geq 2$) are suppressed by the qubit-NAMR nonlinear coupling; so we assume that

$$|C_{2g}|^2 \ll \min\{|C_{0g}|^2, |C_{1g}|^2\}$$

and $|C_{0g}|^2 + |C_{1g}|^2 \simeq 1$. Neglecting C_{2g} in Eq. (24c), we obtain

$$|C_{1g}|^2 = \frac{4\epsilon^2}{8\epsilon^2 + \kappa^2}, \quad (25)$$

and according Eq. (24b), we have

$$|C_{2g}|^2 = \frac{8\epsilon^4}{\left(2\kappa + 4\lambda^2/\Gamma\right)^2\left(8\epsilon^2 + \kappa^2\right)}. \tag{26}$$

These results will be useful to calculate second-order correlation function in the following sections.

B. Sub-Poissonian phonon statistics

The sub-Poissonian phonon statistics can be revealed by measuring the zero-delay-time second-order correlation function

$$g_2(t,0) = \frac{\langle b^\dagger(t)b^\dagger(t)b(t)b(t)\rangle}{\langle b^\dagger(t)b(t)\rangle^2}. \tag{27}$$

We recall that if a given phonon state is described by $g_2(t,0) < 1$ [$g_2(t,0) > 1$], then it exhibits sub-Poissonian (super-Poissonian) phonon statistics, which is also sometimes referred to as phonon antibunching (bunching).

However, here we refer to phonon antibunching and bunching in a more common way, as defined in Sec. IV.B.

Let us denote $g_2(0) = \lim_{t\to\infty} g_2(t,0)$. Then for the state, given by Eq. (21), we find that the correlation function $g_2(0)$ can be expressed by the probability amplitudes as follows

$$g_2(0) \simeq \frac{2|C_{2g}|^2}{|C_{1g}|^4} = \frac{8\epsilon^2 + \kappa^2}{\left(2\kappa + 4\lambda^2\Gamma^{-1}\right)^2}. \tag{28}$$

From Eq. (28), we conclude that, in our second-order nonlinear system, the effective nonlinear coupling strength λ and the qubit decay rate Γ significantly affect the dip of the sub-Poissonian phonon statistics. If a relatively strong coupling strength λ is induced and the relation

$$\frac{4\lambda^2}{\Gamma} \gg \max\{2\sqrt{2}\epsilon, \kappa\} \tag{29}$$

is satisfied, strong sub-Poissonian phonon statistics can be observed in this system with $g_2(0) \ll 1$.

IV. NUMERICAL DESCRIPTION OF PHONON BLOCKADE

A. Steady-state solutions of the master equation

In this section we numerically study the phonon blockade effect via the standard master equation approach. Numerical computations were performed using the Python package QuTiP [62]. We perform numerical calculations in the Fock space of the NAMR of dimension M=10, which is much larger than that assumed in Eq. (21). To verify our analytical results of phonon blockade in Sec. III, we adopt the original Hamiltonian $H_{\rm total}$ in Eq. (7) (not $H_{\rm eff}$) to proceed with our numerical simulations. The Kossakowski-Lindblad master equation for the reduced density matrix $\hat{\rho}(t)$ of the system reads

$$\begin{aligned}\frac{d\hat{\rho}(t)}{dt} &= -i[H_{\rm total}, \hat{\rho}(t)] + D[\sigma_-, \Gamma]\hat{\rho}(t) \\ &\quad + D[\sigma_z, \Gamma_f/2]\hat{\rho}(t) + n_{\rm th}D[b^\dagger, \kappa]\hat{\rho}(t) \\ &\quad + (n_{\rm th}+1)D[b, \kappa]\hat{\rho}(t),\end{aligned} \tag{30}$$

where

$$D[A,\Omega]\hat{\rho} = \frac{1}{2}\Omega(2A\hat{\rho}A^\dagger - A^\dagger A\hat{\rho} - \hat{\rho}A^\dagger A) \tag{31}$$

are Lindblad-form terms, and Γ_f is the pure dephasing rate of the qubit. Recall that Γ corresponds to the qubit decay rate and κ the decay rate of the NAMR. In this proposal, the NAMR might couple to a thermal reservoir of temperature T with thermal phonon number $n_{\rm th} = \{\exp[\hbar\omega_0/(k_BT)] - 1\}^{-1}$, where k_B is the Boltzmann constant.

B. Quantum signatures for steady-state phonon blockade: Phonon antibunching and sub-Poissonian phonon statistics

Here we show that phonon blockade in the infinite-time limit of the dissipative system is also a nonclassical effect because the generated steady-state of the NAMR can exhibit both phonon antibunching and sub-Poissonian phonon statistics.

To reveal phonon antibunching, we apply the steady-state second-order correlation function

$$g_2(t,\tau) = \frac{\langle b^\dagger(t)b^\dagger(t+\tau)b(t+\tau)b(t)\rangle}{\langle b^\dagger(t)b(t)\rangle\langle b^\dagger(t+\tau)b(t+\tau)\rangle}, \tag{32}$$

where τ is the time delay between two measurements. This function reduces to Eq. (27) for τ=0. The two-time correlation function of the steady state of the mechanical mode is the function of only the time delay as given by

$$g_2(\tau) = \lim_{t\to\infty} g_2(t,\tau). \tag{33}$$

Here we refer to phonon antibunching (bunching) for a phonon steady state only if $g_2(\tau) > g_2(0)$ [$g_2(\tau) < g_2(0)$] for a delay time $0 < \tau$, according to the standard definition of these effects [63]. Phonon antibunching also occurs if $g^{(2)}(\tau)$ has a strict local minimum at $\tau = 0$ [64]. Here we only study the phonon antibunching of stationary states. Note that such effect can also be observed for nonstationary cases, but a modification of this definition would be required [64].

Note that these phonon antibunching and bunching effects are defined via two-time phonon-number correlations, while the sub-Poissonian and super-Poissonian statistics are given via single-time phonon-number correlations. So, these are different effects and a given state

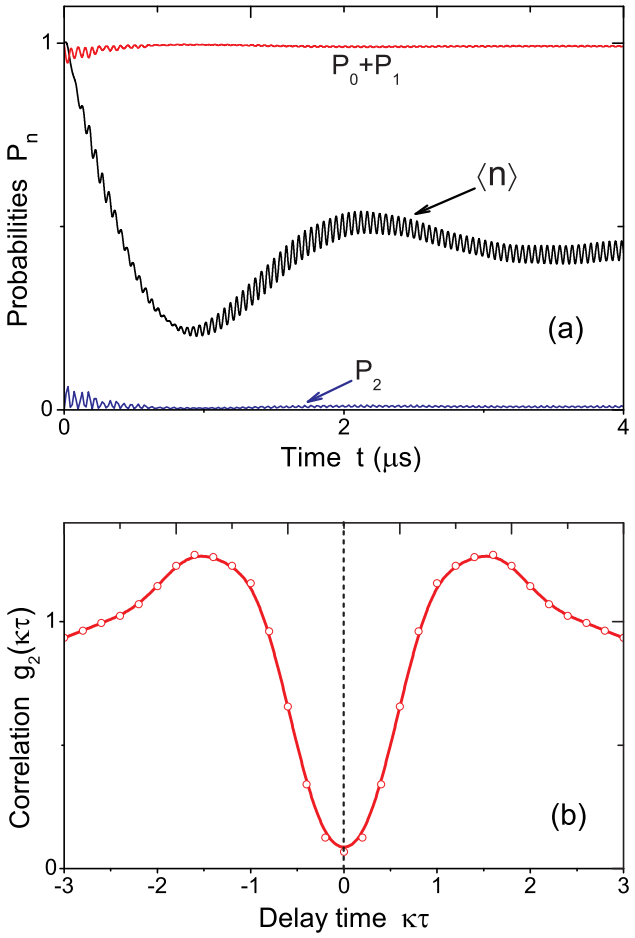

FIG. 3: (Color online) (a) Probabilities P_n of measuring n phonons and the average phonon number $\langle n\rangle$ as a function of the evolution time. (b) Phonon antibunching is revealed by the second-order correlation function versus the rescaled delay time $\kappa\tau$. Other parameters are: $\Gamma/(2\pi) = 1$ MHz, $\Gamma_f = 0$, $\epsilon/(2\pi) = 0.2$ MHz, $\Delta_d = 0$, and $n_{\rm th} = 0$.

of the NAMR can be [65] either (1) both sub-Poissonian and antibunched, or (2) sub-Poissonian and bunched, or (3) super-Poissonian and antibunched, or (4) super-Poissonian and bunched. In this paper we focus on the case (1). Finally, we stress that sub-Poissonian statistics and antibunching are purely nonclassical effects, since they correspond to the violation of classical inequalities [66]. Thus, the observation of either of these effects can be a signature of the quantumness of a NAMR.

In current experiments with a charge qubit and a NAMR, their coupling strength is of orders from tens to hundreds of MHz, as shown in Refs. [67–69]. Moreover, the quality factor of a NAMR at microwave frequencies is around $10^3 \sim 10^5$ [6, 70]. The decay rate of a charge qubit can reach the order of 1 MHz [71]. In the following discussion, we assume that the NAMR oscillates at $\omega_0/(2\pi)$=1 GHz with quality factor Q=5×10^3 [$\kappa/(2\pi) = 0.2$ MHz] and the coupling strength with the qubit is $g/(2\pi) = 80$ MHz. Under the driving rate $\Omega_{\rm p}/(2\pi) = 100$ MHz, the effective nonlinear coupling strength is $\lambda/(2\pi) = 1.28$ MHz. Defining the time-dependent probabilities $P_n(t) = {\rm Tr}[|n\rangle\langle n|\hat{\rho}(t)]$ for the phonon number n and mean phonon number $\langle n\rangle = {\rm Tr}[b^\dagger b\hat{\rho}(t)]$, we have numerically solved the master equation and the results are shown in Fig. 3(a). We find that the sum of P_0 and P_1 is almost one, while P_2 is of an extremely low amplitude, indicating that phonon blockade occurs in this hybrid system. Moreover, the average phonon number $\langle n\rangle$ of the steady-state oscillates around $\sim$0.44, which is due to the high-order terms, as shown in Sec. II.B. In the following numerical results, without loss of generality, we adopt the ensemble-average $\langle n\rangle$ and P_2 of the steady state to calculate $g_2(0)$.

In addition to the time-dependent probabilities $P_n(t)$, other quantum signatures for PB are the phonon intensity correlations with finite-time delays. The delay-time-dependent second-order correlation functions $g_2(\tau)$ are plotted in Fig. 3(b), from which it can be found that if the time delay between two measurements $\kappa\tau$ is within $\sim$1, then a phonon antibunching dip can be observed.

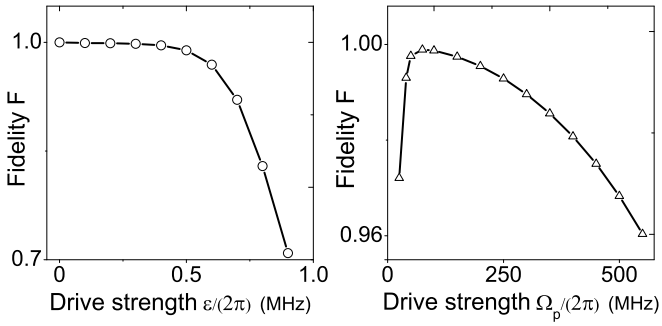

FIG. 4: The fidelity F, given by Eq. (34), of state truncation vs (a) the drive strength ϵ and (b) the effective Rabi frequency $\Omega_{\rm p}$ of the drive field. The other parameters used here are the same as those in Fig. 3(a).

In Sec. III.A, we assumed that the Hilbert space of the system is truncated into its subspace spanned by the four states, given in Eq. (21). This approximation will be not valid if the higher-energy levels are excited. As shown in Ref. [27], we use the fidelity of state truncation to estimate the quality of this effect in a phonon blockade system. With our precise numerical solution obtained in a larger Hilbert space, the fidelity is the sum of the steady-state probabilities of the states considered, which is defined as

$$F(\rho_{ss}) = |C_{0,g}|^2 + |C_{1,g}|^2 + |C_{2,g}|^2 + |C_{0,e}|^2, \qquad (34)$$

where ρ_{ss} is the steady state of the system. The fidelity $F \approx 1$ indicates that we can effectively use these four states to expand the density matrix of the system, and the analytical results in Sec. III are valid. Otherwise, if the fidelity F is much smaller than 1, we can conclude that the higher energy-level beyond these four states are effectively occupied, and it is not enough to use only these four states to describe the system.

In Fig. 4(a), we plot the fidelity F as a function of the drive strength ϵ of the NAMR. With increasing ϵ, the fidelity F does not change much (and remains above 0.99) if $\epsilon/2\pi < 0.5$ MHz. However, if we continue increasing the drive strength ϵ, the fidelity starts to decrease rapidly. In this case, the nonlinear effects cannot effectively prevent multiphonon states being excited. As a result, the phonon blockade effects will be destroyed.

The relation between the fidelity F and the pump strength $\Omega_{\rm p}$ of the qubit is shown in Fig 4(b). We find that the fidelity initially increases rapidly with the pump strength $\Omega_{\rm p}$. This is because the nonlinear strength goes up as shown in Eq. (19). Therefore, blockade effects will be enhanced. However, when $\Omega_{\rm p}/(2\pi)$ increases more than 100 MHz, then the fidelity starts to decrease. This is because the large detuning approximation $\Delta \simeq 2\omega_0 \gg \Omega_{\rm p}$, given by Eq. (16), is not valid any more when $\Omega_{\rm p}$ is too strong. Consequently, the qubit can be effectively excited and the transitions $|g,1\rangle \leftrightarrow |e,1\rangle \leftrightarrow |g,3\rangle$ can occur. Thus, multiphonon states are effectively excited. Moreover, higher-order terms will also deteriorate the fidelity of truncation, as shown in Sec. II.B. It is seen that there is a trade-off when we want to induce the strong nonlinear coupling between the NAMR and the qubit while limiting the strength of the qubit drive to a certain regime.

In Fig. 5, we plot the mean phonon number $\langle n\rangle$ and $g_2(0)$ versus the mechanical drive detuning Δ_d. For a driving force tuned resonantly with the mechanical mode frequency, we observe $g_2(0) \simeq 0.06$. Correspondingly, the average phonon number $\langle n\rangle \approx 0.44$ (according to Eq. (25), the maximum phonon number of the steady state in the PB system is $\langle n\rangle_{\rm max} \simeq 0.5$ assuming $2\sqrt{2}\epsilon \gg \kappa$). Thus, the system can work as an efficient single-phonon source device with a large output of phonons. When increasing the detuning Δ_d, $g_2(0)$ rises, while the mean phonon number $\langle n\rangle$ decreases, and around $\Delta_d \simeq \pm\sqrt{2}\lambda/2$ two small bunching peaks [$g_2(0) \sim 5$] can be observed due to resonantly driving the second excited states [see Fig. 2(c)].

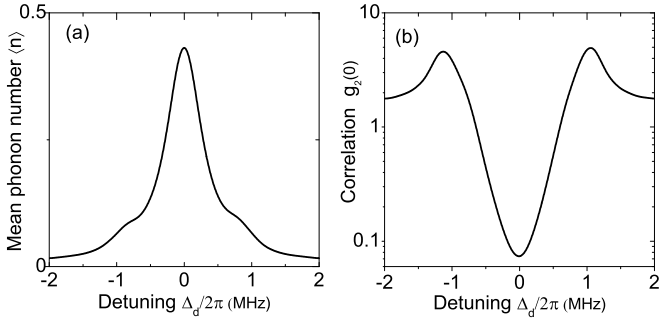

FIG. 5: (a) Mean phonon number $\langle n\rangle$, and (b) zero-delay time second-order correlation function $g_2(0)$ as functions of the frequency detuning $\Delta_d/(2\pi)$ of the driving force.

C. Discussions on increasing the robustness

Equation (28) indicates that PB strongly depends on the ratio $4\lambda^2/\Gamma$. Once the relation Eq. (29) is not valid, phonon antibunching in this hybrid system might not occur. In Fig. 6(a) we show how $g_2(0)$ depends on Γ and the nonlinear coupling strength λ (during the numerical simulations, λ is adjusted by changing the drive strength). From the results in Fig. 6(a), it can be found that PB is preserved under the drive strength $\Omega_{\rm p}/(2\pi) = 200$ MHz [$\lambda/(2\pi) = 2.56$ MHz, the blue solid curve in Fig. 6(a)] with $g_2(0) \simeq 0.07$, even when $\Gamma/2\pi$ increases to 6 MHz. However, when $\Omega_{\rm p}/2\pi$ decreases to 50 MHz [$\lambda/(2\pi) = 0.64$ MHz, the red-dashed curve in Fig. 6(a)], $2\sqrt{2}\epsilon$ and κ are comparable to $4\lambda^2/\Gamma$ when $\Gamma/(2\pi)$ exceeds ~ 3 MHz, and phonon antibunching is more fragile to the rapid decay rate of the qubit. We conclude that the strong drive strength can increase the robustness of the PB against the rapid decay of the qubit.

The thermal phonons in the environment can also destroy PB to some extent. To beat the thermal noise, one can increase the induced nonlinearity of this PB system, or employ the NAMR of a high-quality factor. Here we set the quality factor Q as 5×10^3 and 5×10^4, respectively, and plot two curves describing $g_2(0)$ as a function of $n_{\rm th}$ in Fig. 6(b). For $Q=5\times10^3$, $g_2(0)$ is almost ~ 2 when the thermal phonon number increases to $n_{\rm th} = 2$, indicating that the NAMR is described by the super-Poissonian distribution due to the thermal noise. However, under $Q=5\times10^4$, $g_2(0)$ rises much slower with increasing $n_{\rm th}$. To observe better PB without being destroyed by the thermal phonons, we can employ a high-quality factor NAMR to decouple it from the thermal environment.

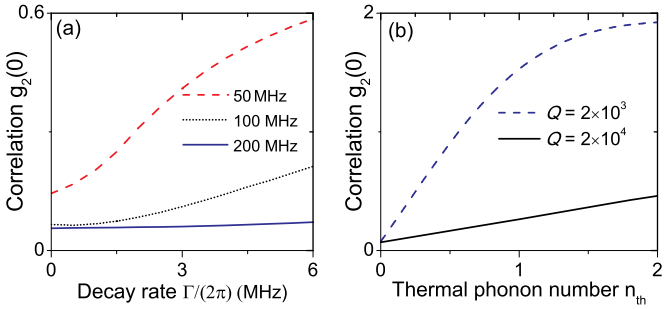

FIG. 6: (Color online) (a) Dependence of the sub-Poissonian dip $g_2(0)$ on the decay rate of the qubit, for different values of the driving strength $\Omega_{\rm p}/(2\pi) = 50$ MHz (red dashed curve), $\Omega_{\rm p}/(2\pi) = 100$ MHz (black dot curve) and $\Omega_{\rm p}/(2\pi) = 200$ MHz (blue solid curve). (b) $g_2(0)$ vs thermal phonon number $n_{\rm th}$ for different values of the quality factor $Q = 5\times10^3$ (blue dashed curve) and $Q = 5\times10^4$ (black solid curve). The other parameters used here are the same as those in Fig. 3(a).

So far we have not considered the effect of pure dephasing of the qubit. In Fig. 7, we show the second-order correlation function $g_2(\tau)$ under different values of the pure dephasing rate Γ_f. We find that the rapid de-

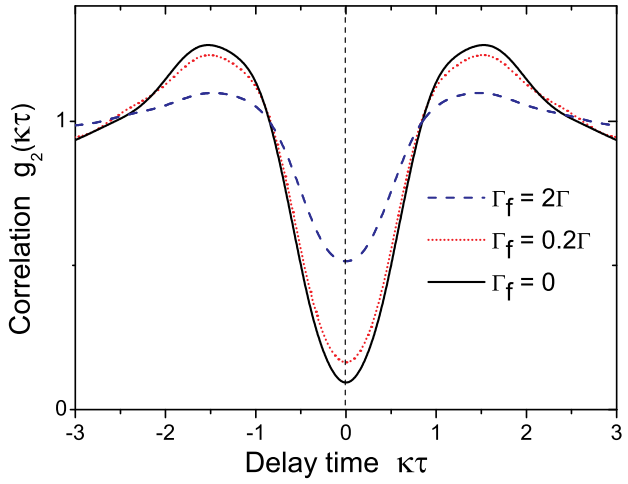

FIG. 7: (Color online) Steady-state second-order correlation function g_2 of the mechanical mode versus the rescaled delay time $\kappa\tau$, assuming various values of the pure-dephasing rate $\Gamma_f = 0$ (black solid curve), $\Gamma_f = 0.2\Gamma$ (red dot curve), $\Gamma_f = 2\Gamma$(blue dashed curve), where Γ is the qubit decay rate and κ is the decay rate of the NAMR. Here the other parameters are the same as those in Fig. 3(a).

phasing rate will destroy the blockade effects; but even when $\Gamma_f = 2\Gamma$, $g_2(0)$ is still about 0.5, indicating that the NAMR still exhibits phonon antibunching. In experimental implementations, to minimize the dephasing noise, the qubit should be operated around its degeneracy point, and the dephasing time has been measured even longer than 500 ns [i.e., $\Gamma_f/(2\pi) \sim 0.3$ MHz] as reported in Ref. [72]. Alternatively, by coupling the mechanical mode to the SQUID loop, we can also obtain a strong coupling of a linear longitudinal form, which has been demonstrated in Refs. [9, 55]. With the tunneling energy being in the dominant position and at the degeneracy point, the dephasing due to charge fluctuations can also be minimized. Another approach is to improve the properties of the Josephson junctions and materials to eliminate excess sources of $1/f$ noise [73, 74]. All these strategies will increase the dephasing time significantly, and the effect of pure dephasing of the qubit can effectively be suppressed.

V. DETECTING PHONON BLOCKADE BY MEASURING THE QUBIT

Another challenge for phonon blockade is its detection. In Ref. [23], the authors demonstrated that, in principle, PB could be measured via the power spectrum of the induced electromotive force between the two ends of the NAMRs: the observation of extra peaks in the power spectrum means the deterioration of PB. Another detecting method has been shown in Ref. [24]: With the NAMR resonantly coupled with a microwave resonator cavity, the photons in the cavity will be entangled with phonons, and they will share the same dynamics. If detections of photons indicate photon blockade, we can conclude that the NAMR is in a PB state. In this induced second-order nonlinear system, the detection might be easier: energy exchanging via the nonlinear term makes it possible to obtain the information of the NAMR by detecting the qubit.

For single-PB systems, the most important signature is the small probability of the incoming second phonon. Under low-power driving for the qubit and NAMR, the probabilities P_e and P_2 (denoting the qubit in its excited state and the NAMR in the Fock state $|2\rangle$), are approximately equal to P_{0e} and P_{2g}, respectively; that is, $P_e \simeq P_{0e}$ and $P_2 \simeq P_{2g}$. Due to the effective nonlinear coupling between the NAMR and the qubit, there is a coherent transition $|e,0\rangle \leftrightarrow |g,2\rangle$ and the relation between P_{0e} and P_{2g} of the steady states under the weak driving $\epsilon \ll \lambda$ is given in Eq. (24a): P_{2g} is proportional to P_{0e}. Thus, we can measure P_e to estimate the population of the second phonon being excited, and the sensitivity of this detection is decided by the amount $(\lambda/\Gamma)^2$: for larger $(\lambda/\Gamma)^2$, the smaller $|C_{2g}|^2$ will lead to a larger probability of the qubit in its excited state. In Fig. 8, we plot both P_e and P_2 as a function of $g_2(0)$, and these quantities are changed by increasing the drive ϵ. From Fig. 8(a), it can be found that when strong sub-Poissonian phonon statistics is observed [$g_2(0) \simeq 0.07$], both P_2 and P_e are of extremely low amplitude. When $g_2(0)$ starts to rise, P_2 and P_e increase very rapidly. Thus, the observation of the qubit in its excited state can be a signature of imperfect single-PB, and a higher probability P_e indicates a worse phonon blockade effect for the NAMR.

In Fig. 8(b), we set the driving strength of the qubit $\Omega_p/(2\pi)$ equal to 100 MHz and 200 MHz, respectively, and define the ratio $R = P_e/P_2$ to estimate the sensitivity: a large ratio R means that this detection is more sensitive. We find that for a stronger drive, R is always much higher than that of the weaker drive case. We conclude that the large effective coupling strength does not only benefit the robustness against environmental noise, but also increases the sensitivity of the PB measurement.

VI. CONCLUSION

We have shown how to observe phonon blockade induced by the effective nonlinear coupling between a charge qubit and an NAMR. This coupling could be realized in the hybrid system shown in Fig. 1. In this composite system, phonon blockade effects will occur under resonant driving for the NAMR. By analyzing the solution of the system steady states, we have obtained the conditions for strong phonon antibunching and sub-Poissonian phonon statistics. Specifically, the ratio $4\lambda^2/\Gamma$ must exceed the phonon decay rate κ and the driving force strength ϵ.

In the numerical section, we have discussed how to more efficiently observe phonon blockade in our proposal:

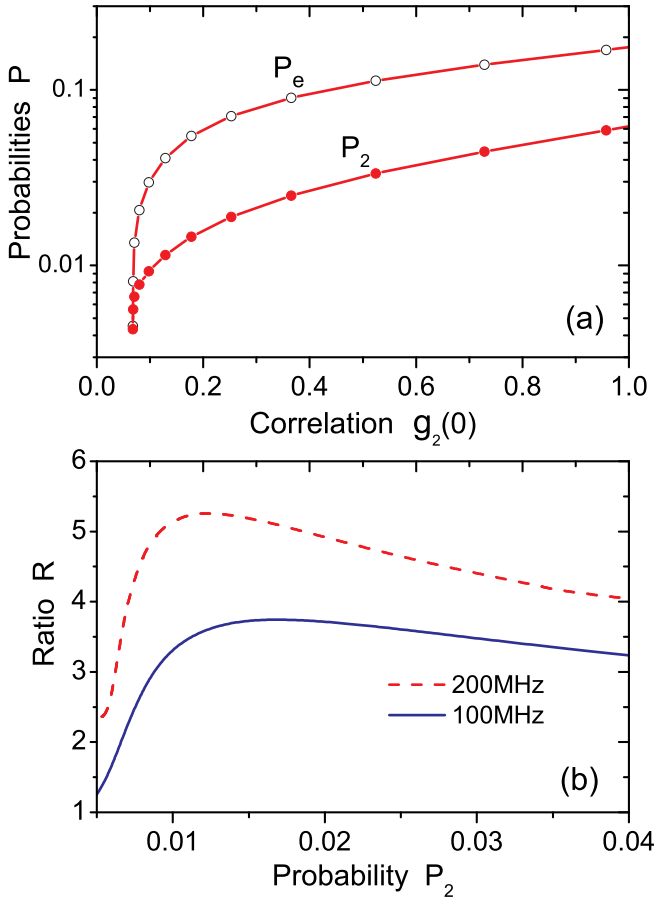

FIG. 8: (Color online) (a) Probabilities $P_e \simeq |C_{0e}|^2$ and $P_2 \simeq |C_{2g}|^2$, as defined in Eq. (21), as a function the zero-delay-time second-order correlation function $g_2(0)$ under the driving strength $\Omega_p/(2\pi) = 100$ MHz. (b) Ratio $R = P_e/P_2$ versus P_2. Here we set $\Omega_p/(2\pi)$ equals to 100 MHz (blue solid curve) and 200 MHz (red dashed curve). The other parameters used here are the same as those in Fig. 3(a).

(1) A relatively strong nonlinear coupling λ should be induced, which can increase the robustness of phonon blockade against different types of noise. This could be realized by increasing the strength of the driving field (or the longitudinal coupling strength); but both driving and coupling strengths should be controlled within certain regimes to avoid the rapid oscillating terms from destroying the blockade. (2) The dephasing noise of the qubit should be suppressed, and the temperature should be low enough so that thermal phonons are negligible. For a NAMR oscillating at several GHz, the thermal occupation number will be about 10^{-3} at temperatures $\sim$10 mK, which is within the capability of dilution refrigerators. (3) The quality factor Q of the NAMR should be high enough to guarantee that the mechanical mode decouples from the thermal environment.

Moreover, we have shown how to use the qubit as a detector to check the imperfections of PB. The numerical results indicate that the sensitivity of this detection can benefit from the strong nonlinear coupling between the NAMR and the qubit. Besides engineering the NAMR into PB states, the induced second-order nonlinearity in our proposal can also be used to demonstrate some other quantum effects of mechanical motions, such as squeezing and superposition states (Schrödinger cat-like states) [8, 55]. All parameters in our proposal are within experimentally accessible regimes, so it might be an efficient method to observe quantum features of nanomechanical motions.

Acknowledgments

X.W. is supported by the China Scholarship Council (Grant No. 201506280142). F.N. is partially supported by the RIKEN iTHES Project, the IMPACT program of JST, and a Grant-in-Aid for Scientific Research (A). We acknowledge the support of a grant from the John Templeton Foundation.

[1] M. D. LaHaye, O. Buu, B. Camarota, and K. C. Schwab, Approaching the quantum limit of a nanomechanical resonator, Science **304**, 74 (2004).
[2] M. Blencowe, Quantum electromechanical systems, Phys. Rep. **395**, 159 (2004).
[3] K. C. Schwab and M. L. Roukes, Putting mechanics into quantum mechanics, Phys. Today **58**, 36 (2005).
[4] M. Poot and H. S. J. van der Zant, Mechanical systems in the quantum regime, Phys. Rep. **511**, 273 (2012).
[5] M. Aspelmeyer, T. J. Kippenberg, and F. Marquard, Cavity optomechanics, Rev. Mod. Phys. **86**, 1391 (2014).
[6] J. D. Teufel, T. Donner, D. Li, J. W. Harlow, M. S. Allman, K. Cicak, A. J. Sirois, J. D. Whittaker, and R. W. Simmonds, Sideband cooling of micromechanical motion to the quantum ground state, Nature (London) **475**, 359 (2011).
[7] Z.-Q. Yin, T. Li, X. Zhang, and L. M. Duan, Large quantum superpositions of a levitated nanodiamond through spin-optomechanical coupling, Phys. Rev. A **88**, 033614 (2013).
[8] H. Tan, F. Bariani, G. Li, and P. Meystre, Generation of macroscopic quantum superpositions of optomechanical oscillators by dissipation, Phys. Rev. A **88**, 023817 (2013).
[9] F. Xue, Y. X. Liu, C. P. Sun, and F. Nori, Two-mode squeezed states and entangled states of two mechanical resonators, Phys. Rev. B **76**, 064305 (2007).
[10] H. Seok, L. F. Buchmann, S. Singh, S. K. Steinke, and P. Meystre, Generation of mechanical squeezing via magnetic dipoles on cantilevers, Phys. Rev. A **85**, 033822 (2012).
[11] J. M. Pirkkalainen, E. Damskägg, M. Brandt, F. Mas-

sel, and M. A. Sillanpää, Squeezing of Quantum Noise of Motion in a Micromechanical Resonator, Phys. Rev. Lett. **115**, 243601 (2015).

[12] X. M. H. Huang, C. A. Zorman, M. Mehregany, and M. L. Roukes, Nanodevice motion at microwave frequencies, Nature (London) **421**, 496 (2003).

[13] F. Marquardt, J. P. Chen, A. A. Clerk, and S. M. Girvin, Quantum theory of cavity-assisted sideband cooling of mechanical motion, Phys. Rev. Lett. **99**, 093902 (2007).

[14] F. Xue, Y. Wang, Y.-X. Liu, and F. Nori, Cooling a micromechanical beam by coupling it to a transmission line, Phys. Rev. B **76**, 205302 (2007).

[15] M. Grajcar, S. Ashhab, J. Johansson, and F. Nori, Lower limit on the achievable temperature in resonator-based sideband cooling, Phys. Rev. B **78**, 035406 (2008).

[16] M. Poggio, C. L. Degen, H. J. Mamin, and D. Rugar, Feedback cooling of a cantilever's fundamental mode below 5 mK, Phys. Rev. Lett. **99**, 017201 (2007).

[17] J. Zhang, Y.-X. Liu, and F. Nori, Cooling and squeezing the fluctuations of a nanomechanical beam by indirect quantum feedback control, Phys. Rev. A **79**, 052102 (2009).

[18] T. J. Kippenberg and K. J. Vahala, Cavity optomechanics: Back-action at the mesoscale, Science **321**, 1172 (2008).

[19] Z.-L. Xiang, S. Ashhab, J. Q. You, and F. Nori, Hybrid quantum circuits: Superconducting circuits interacting with other quantum systems, Rev. Mod. Phys. **85**, 623 (2013).

[20] W. Xiong, D.-Y. Jin, J. Jing, C.-H. Lam, and J. Q. You, Controllable coupling between a nanomechanical resonator and a coplanar-waveguide resonator via a superconducting flux qubit, Phys. Rev. A **92**, 032318 (2015).

[21] M. J. Woolley, G. J. Milburn, and C. M. Caves, Nonlinear quantum metrology using coupled nanomechanical resonators, New J. Phys. **10**, 125018 (2008).

[22] B. Arash, J. W. Jiang, and T. Rabczuk, A review on nanomechanical resonators and their applications in sensors and molecular transportation, Appl. Phys. Rev. **2**, 021301 (2015).

[23] Y.-X. Liu, A. Miranowicz, Y. B. Gao, J. Bajer, C. P. Sun, and F. Nori, Qubit-induced phonon blockade as a signature of quantum behavior in nanomechanical resonators, Phys. Rev. A **82**, 032101 (2010).

[24] N. Didier, S. Pugnetti, Y. M. Blanter, and R. Fazio, Detecting phonon blockade with photons, Phys. Rev. B **84**, 054503 (2011).

[25] A. Miranowicz, J. Bajer, N. Lambert, Y.-X. Liu, F. Nori, Tunable multiphonon blockade in coupled nanomechanical resonators, Phys. Rev. A **93**, 013808 (2016).

[26] A. Imamoglu, H. Schmidt, G. Woods, and M. Deutsch, Strongly interacting photons in a nonlinear cavity, Phys. Rev. Lett. **79**, 1467 (1997).

[27] A. Miranowicz, M. Paprzycka, Y. X. Liu, J. Bajer, and F. Nori, Two-photon and three-photon blockades in driven nonlinear systems, Phys. Rev. A **87**, 023809 (2013).

[28] Y. X. Liu, X. W. Xu, A. Miranowicz, and F. Nori, From blockade to transparency: Controllable photon transmission through a circuit-QED system, Phys. Rev. A **89**, 043818 (2014).

[29] X. W. Xu and Y. Li, Tunable photon statistics in weakly nonlinear photonic molecules, Phys. Rev. A **90**, 043822 (2014).

[30] Y. H. Zhou, H. Z. Shen, and X. X. Yi, Unconventional photon blockade with second-order nonlinearity, Phys. Rev. A **92**, 023838 (2015).

[31] Y.-L. Liu, G.-Z. Wang, Y.-X. Liu, and F. Nori, Mode coupling and photon antibunching in a bimodal cavity containing a dipole quantum emitter, Phys. Rev. A **93**, 013856 (2016).

[32] A. Miranowicz, W. Leoński, and N. Imoto, Quantum-optical states in finite-dimensional Hilbert space. I. General formalism, Adv. Chem. Phys. **119**, 155 (2001); W. Leoński and A. Kowalewska-Kudlaszyk, Quantum scissors: Finite-dimensional states engineering, Prog. Opt. **56**, 131 (2011).

[33] K. M. Birnbaum, A. Boca, R. Miller, A. D. Boozer, T. E. Northup, and H. J. Kimble, Photon blockade in an optical cavity with one trapped atom, Nature (London) **436**, 87 (2005).

[34] N. Lambert and F. Nori, Detecting quantum-coherent nanomechanical oscillations using the current-noise spectrum of a double quantum dot, Phys. Rev. B **78**, 214302 (2008).

[35] A. Majumdar and D. Gerace, Single-photon blockade in doubly resonant nanocavities with second-order nonlinearity, Phys. Rev. B **87**, 235319 (2013).

[36] H. Z. Shen, Y. H. Zhou, and X. X. Yi, Quantum optical diode with semiconductor microcavities, Phys. Rev. A **90**, 023849 (2014).

[37] J. Tang, W. Geng, and X. Xu, Quantum Interference Induced Photon Blockade in a Coupled Single Quantum Dot-Cavity System, Sci. Rep. **5**, 9252 (2015).

[38] W. Leoński and A. Miranowicz: Kerr nonlinear coupler and entanglement, J. Optics B **6**, S37 (2004); A. Miranowicz and W. Leoński, Two-mode optical state truncation and generation of maximally entangled states in pumped nonlinear couplers, J. Phys. B **39**, 1683 (2006).

[39] T. C. H. Liew and V. Savona, Single Photons from Coupled Quantum Modes, Phys. Rev. Lett. **104**, 183601 (2010).

[40] H. Flayac and V. Savona, Input-output theory of the unconventional photon blockade, Phys. Rev. A **88**, 033836 (2013).

[41] D. Gerace and V. Savona, Unconventional photon blockade in doubly resonant microcavities with second-order nonlinearity, Phys. Rev. A **89**, 031803 (2014).

[42] M.-A. Lemonde, N. Didier, and A. A. Clerk, Antibunching and unconventional photon blockade with Gaussian squeezed states, Phys. Rev. A **90**, 063824 (2014).

[43] J. R. Johansson, N. Lambert, I. Mahboob, H. Yamaguchi, and F. Nori, Entangled-state generation and Bell inequality violations in nanomechanical resonators, Phys. Rev. B **90**, 174307 (2014).

[44] Y. Makhlin, G. Schon, and A. Shnirman, Quantum-state engineering with Josephson-junction devices, Rev. Mod. Phys. **73**, 357 (2001).

[45] J. Q. You and F. Nori, Atomic physics and quantum optics using superconducting circuits, Nature (London) **474**, 589 (2011).

[46] Y.-D. Wang, A. Kemp, and K. Semba, Coupling superconducting flux qubits at optimal point via dynamic decoupling with the quantum bus, Phys. Rev. B **79**, 024502 (2009).

[47] A. J. Kerman, Quantum information processing using quasiclassical electromagnetic interactions between qubits and electrical resonators, New J. Phys. **15**, 123011 (2013).

[48] N. Didier, J. Bourassa, and A. Blais, Fast Quantum Nondemolition Readout by Parametric Modulation of Longitudinal Qubit-Oscillator Interaction, Phys. Rev. Lett. **115**, 203601 (2015).

[49] C. Wilson, G. Johansson, T. Duty, F. Persson, M. Sandberg, and P. Delsing, Dressed relaxation and dephasing in a strongly driven two-level system, Phys. Rev. B **81**, 024520 (2010).

[50] Y. X. Liu, C. X. Yang, H. C. Sun, and X. B. Wang, Coexistence of single- and multi-photon processes due to longitudinal couplings between superconducting flux qubits and external fields, New J. Phys. **16**, 015031 (2014).

[51] Y. J. Zhao, Y. L. Liu, Y. X. Liu, and F. Nori, Generating nonclassical photon states via longitudinal couplings between superconducting qubits and microwave fields, Phys. Rev. A **91**, 053820 (2015).

[52] L. Garziano, R. Stassi, V. Macrì, A. F. Kockum, S. Savasta, and F. Nori, Multiphoton quantum Rabi oscillations in ultrastrong cavity QED, Phys. Rev. A **92**, 063830 (2015).

[53] J. Zhang, B. Peng, Ş. K. Özdemir, Y.-X. Liu, H. Jing, X.-Y. Lü, Y.-l. Liu, L. Yang, and F. Nori, Giant nonlinearity via breaking parity-time symmetry: A route to low-threshold phonon diodes, Phys. Rev. B **92**, 115407 (2015).

[54] X.-Y. Lü, J. Q. Liao, L. Tian, and F. Nori, Steady-state mechanical squeezing in an optomechanical system via Duffing nonlinearity, Phys. Rev. A **91**, 013834 (2015).

[55] X. X. Zhou and A. Mizel, Nonlinear coupling of nanomechanical resonators to Josephson quantum circuits, Phys. Rev. Lett. **97**, 267201 (2006).

[56] A. D. Armour, M. P. Blencowe, and K. C. Schwab, Entanglement and decoherence of a micromechanical resonator via coupling to a Cooper-pair box, Phys. Rev. Lett. **88**, 148301 (2002).

[57] E. K. Irish and K. Schwab, Quantum measurement of a coupled nanomechanical resonator-Cooper-pair box system, Phys. Rev. B **68**, 155311 (2003).

[58] C. P. Sun, L. F. Wei, Y. X. Liu, and F. Nori, Quantum transducers: Integrating transmission lines and nanomechanical resonators via charge qubits, Phys. Rev. A **73**, 022318 (2006).

[59] I. Wilson-Rae, P. Zoller, and A. Imamoglu, Laser cooling of a nanomechanical resonator mode to its quantum ground state, Phys. Rev. Lett. **92**, 075507 (2004).

[60] I. Wilson-Rae, C. Galland, W. Zwerger, and A. Imamoglu, Exciton-assisted optomechanics with suspended carbon nanotubes, New J. Phys. **14**, 115003 (2012).

[61] P. Rabl, P. Cappellaro, M. G. Dutt, L. Jiang, J. Maze, and M. D. Lukin, Strong magnetic coupling between an electronic spin qubit and a mechanical resonator, Phys. Rev. B **79**, 041302 (2009).

[62] J. Johansson, P. Nation, and F. Nori, QuTiP 2: A Python framework for the dynamics of open quantum systems, Comput. Phys. Commun. **184**, 1234 (2013).

[63] L. Mandel and E. Wolf, *Optical Coherence and Quantum Optics* (Cambridge Univ. Press, Cambridge, UK, 1995).

[64] A. Miranowicz, J. Bajer, H. Matsueda, M. R. B. Wahiddin and R. Tanaś, Comparative study of photon antibunching of non-stationary fields (part I), J. Opt. B: Quantum Semiclass. Opt. **1**, 511 (1999); A. Miranowicz, H. Matsueda, J. Bajer, M. R. B. Wahiddin and R. Tanaś, Comparative study of photon bunching of classical fields (part II), J. Opt. B: Quantum Semiclass. Opt. **1**, 603 (1999).

[65] X. T. Zou and L. Mandel, Photon-antibunching and sub-Poissonian photon statistics, Phys. Rev. A **41**, 475 (1990).

[66] A. Miranowicz, M. Bartkowiak, X. Wang, Y. X. Liu, and F. Nori, Testing nonclassicality in multimode fields: A unified derivation of classical inequalities, Phys. Rev. A **82**, 013824 (2010).

[67] I. Martin, A. Shnirman, L. Tian, and P. Zoller, Ground-state cooling of mechanical resonators, Phys. Rev. B **69**, 125339 (2004).

[68] P. Rabl, A. Shnirman, and P. Zoller, Generation of squeezed states of nanomechanical resonators by reservoir engineering, Phys. Rev. B **70**, 205304 (2004).

[69] L. Tian, Entanglement from a nanomechanical resonator weakly coupled to a single Cooper-pair box, Phys. Rev. B **72**, 195411 (2005).

[70] J. A. Sidles, J. L. Garbini, K. J. Bruland, D. Rugar, O. Züger, S. Hoen, and C. S. Yannoni, Magnetic-Resonance Force Microscopy, Rev. Mod. Phys. **67**, 249 (1995).

[71] D. I. Schuster et al., Resolving photon number states in a superconducting circuit, Nature (London) **445**, 515 (2007).

[72] D. Vion, A. Aassime, A. Cottet, P. Joyez, H. Pothier, C. Urbina, D. Esteve, and M. H. Devoret, Manipulating the Quantum State of an Electrical Circuit, Science **296**, 886 (2002).

[73] J. Koch, T. M. Yu, J. Gambetta, A. A. Houck, D. I. Schuster, J. Majer, A. Blais, M. H. Devoret, S. M. Girvin, and R. J. Schoelkopf, Charge-insensitive qubit design derived from the Cooper pair box, Phys. Rev. A **76**, 042319 (2007).

[74] J. M. Martinis, K. B. Cooper, R. McDermott, M. Steffen, M. Ansmann, K. D. Osborn, K. Cicak, S. Oh, D. P. Pappas, R. W. Simmonds, and C. C. Yu, Decoherence in Josephson Qubits from Dielectric Loss, Phys. Rev. Lett. **95**, 210503 (2005).